Monthly Notices of the ROYAL ASTRONOMICAL SOCIETY

MNRAS **482,** 2294–2304 (2019) doi:10.1093/mnras/sty2703

High-resolution VLA observations of FR0 radio galaxies: the properties and nature of compact radio sources

Ranieri D. Baldi [1]★ Alessandro Capetti[2] and Gabriele Giovannini[3,4]

[1] *School of Physics and Astronomy, University of Southampton, Southampton SO17 1BJ, UK*
[2] *INAF – Osservatorio Astrofisico di Torino, Strada Osservatorio 20, I-10025 Pino Torinese, Italy*
[3] *Dipartimento di Fisica e Astronomia, Università di Bologna, via Gobetti 93/2, I-40129 Bologna, Italy*
[4] *INAF – Istituto di Radio Astronomia, via P. Gobetti 101, I-40129 Bologna, Italy*

Accepted 2018 October 2. Received 2018 October 2; in original form 2018 July 18

ABSTRACT

We present the results of Karl G. Jansky Very Large Array (VLA) observations regarding the properties of FR0 radio galaxies, the compact radio sources associated with early-type galaxies that represent the bulk of the local radio-loud population of active galactic nuclei. We obtained A-array observations at 1.5, 4.5 and 7.5 GHz for 18 FR0s from the FR0*CAT* sample: these are sources at $z < 0.05$, which are unresolved in the FIRST images and spectroscopically classified as low-excitation galaxies (LEGs). Although we reach an angular resolution of ∼0.3 arcsec, the majority of the 18 FR0s are still unresolved. Only four objects show extended emission. Six have steep radio spectra, 11 have flat cores, while one shows an inverted spectrum. We find that (i) the ratio between the core and total emission in FR0s is ∼30 times higher than that in FRIs, and (ii) FR0s have the same properties as FRIs from the nuclear and host points of view. FR0s differ from FRIs only in the paucity of extended radio emission. Various evolutionary scenarios were investigated: (i) the possibility that all FR0s are young sources eventually evolving into extended sources was ruled out by the distribution of radio sizes; (ii) similarly, a time-dependent scenario, in which a variation of accretion or jet launching prevents the formation of large-scale radio structures, appears to be implausible owing to the large abundance of subkiloparsec objects; (iii) a scenario in which FR0s are produced by mildly relativistic jets is consistent with the data but requires observations of a larger sample if it is to be properly tested.

Key words: galaxies: active – galaxies: elliptical and lenticular, cD – galaxies: jets – galaxies: nuclei – radio continuum: galaxies.

1 INTRODUCTION

Among the variety of observed morphologies of radio-emitting active galactic nuclei (AGNs) in the local Universe, the most common one is the presence of a single compact emitting region (Baldi & Capetti 2010). This conclusion could be drawn only after the advent of deep large-area radio surveys in opposition to the general results obtained from high-flux limited sample studies (such as the 3C, 2Jy and B2 catalogues, Bennett 1962; Wall & Peacock 1985; Colla et al. 1975), which typically selected radio sources extending on scales of many kiloparsecs and belonging to the Fanaroff & Riley classes I and II. The cross-match of optical and radio surveys (SDSS, NVSS and FIRST data set, SDSS/NVSS sample, Best et al. 2005; Best & Heckman 2012) showed that compact radio sources, at 5-arcsec resolution, represent the vast majority of the local radio AGN population (Baldi & Capetti 2009, 2010; Sadler et al. 2014; Banfield & al. 2015; Whittam et al. 2016, 2017; Miraghaei & Best 2017; Lukic et al. 2018). Earlier radio studies (Rogstad & Ekers 1969; Heeschen 1970; Ekers & Ekers 1973; Wrobel & Heeschen 1991; Slee et al. 1994; Giroletti, Giovannini & Taylor 2005) had pointed out that most of the radio sources in the local Universe are flat-spectrum compact sources, but the attention of the community has focused mainly on the study of extended radio sources (FRI/FRII).

Compact radio sources can potentially be associated with different classes of AGNs, including radio-quiet AGNs, compact steep-spectrum sources (CSSs) and blazars. By using multiwavelength data provided by SDSS, Baldi & Capetti (2010) selected from the SDSS/NVSS sample (Best et al. 2005; Best & Heckman 2012) a large population of massive red early-type galaxies (ETGs) associated with compact radio sources. These objects have been named FR0s by Ghisellini (2011) as a convenient way of linking the compact radio sources seen in nearby galaxies with

★ E-mail: R.Baldi@soton.ac.uk

the canonical Fanaroff–Riley classification scheme (Sadler et al. 2014). Adopting these selection criteria, FR0s form a fairly homogeneous population of low-luminosity radio galaxies (Baldi, Capetti & Massaro 2018a). FR0s appear indistinguishable from low-power FRI/FRII low-excitation galaxy (LEG) radio sources (Capetti, Massaro & Baldi 2017a,b), displaying a similar range of AGN bolometric luminosities, host galaxy properties and black hole (BH) masses: it seems that the only feature that distinguishes FR0s from the other FR classes is their lack of substantial extended radio emission.

Because this vast population is still virtually unexplored, Baldi, Capetti & Giovannini (2015) carried out a pilot study of the Karl G. Jansky Very Large Array (VLA) radio imaging of a small sample of FR0s. The main result is that most of the sources still appear compact at higher resolution, with ∼80 per cent of the total radio emission unresolved in the core (i.e. they are highly core-dominated). The few extended sources show a symmetric radio structure. Their radio spectra generally are flat or steep, but with an emerging flat core at higher radio frequencies. In addition, these sources show radio-core energetics, line and X-ray luminosities (Torresi et al. 2018) that are similar to those of FRIs . Baldi et al. (2015) concluded that FR0s are able to launch a jet whose unresolved radio-core base appears indistinguishable from those of FRIs but that is not emitting prominently at large scales. This radio behaviour is similar to what is observed in nearby giant ETGs which harbour low-power radio-loud AGNs (10^{36-38} erg s^{-1}; Baldi & Capetti 2009; Baldi, Capetti & Giovannini 2016), termed Core Galaxies (CoreG, Balmaverde & Capetti 2006) or very low-power (10^{33-38} erg s^{-1}) low-ionization nuclear emitting-line regions (LINERs) recently studied with eMERLIN (Baldi et al. 2018b) and VLA array (Nyland et al. 2016). These sources exhibit compact radio emission at the VLA resolution, which is only occasionally associated with diffuse extended emission (Filho, Barthel & Ho 2000, 2002; Falcke et al. 2000; Nagar et al. 2000, 2002), and is consistent with a FR0 classification.

The multiband properties of FR0s indicate that their compactness and high core dominance are genuine and not due to a geometric effect (Baldi et al. 2015; Torresi et al. 2018). All these characteristics point to the uniqueness of the radio properties of the FR0s as a standalone class, different from the other FR classes, blazars, CSSs and radio-quiet AGNs.

We proposed various explanations to account for the radio properties of FR0s. Their small size might indicate the youth of their radio activity, but Baldi et al. (2018a) showed that a scenario in which all FR0s eventually evolve into extended radio sources cannot account for the space numbers of the various FR classes. However, other open possibilities are as follows: (i) FR0s could be short-lived and/or recurrent episodes of AGN activity, which are not long enough for radio jets to develop at large scales (Sadler et al. 2014); (ii) FR0s could produce slow jets, possibly owing to low BH spin, which then experience instabilities and entrainment in the dense interstellar medium of the host galaxy corona that cause their premature disruption (Baldi & Capetti 2009; Bodo et al. 2013); and (iii) the differences between FR0s and extended radio galaxies could be caused by their distinct environments.

In order to explore FR0s with a more systematic approach, we selected a homogeneous and well-defined sample of such sources, named FR0*CAT* (Baldi et al. 2018a). FR0*CAT* includes 104 compact radio sources selected by combining observations from the NVSS, FIRST and SDSS surveys (see Appendix A for an update of the catalogue). We included in the catalogue those sources with redshift $\leq$0.05 and with an optical spectrum characteristic of low-excitation galaxies. We imposed a limit on their deconvolved angular sizes of 4 arcsec, corresponding to a linear size of $\lesssim$5 kpc, based on the FIRST images. Their FIRST radio luminosities at 1.4 GHz are mostly in the range $10^{38} \lesssim \nu L_{1.4} \lesssim 10^{40}$ erg s^{-1}. The FR0*CAT* hosts are mostly (86 per cent) luminous ($-21 \gtrsim M_r \gtrsim -23$) red early-type galaxies with BH masses of $10^8 \lesssim M_{\rm BH} \lesssim 10^9$ M$_\odot$, with a small tail down to $10^{7.5}$ M$_\odot$.

Compactness is not a well-defined property, as it depends on the resolution, sensitivity and frequency of the available observations. Furthermore, we lack any information on the radio spectral shape of the FR0 sources. For these reasons, we started a comprehensive study of FR0*CAT* sources with VLA observations at a higher frequency and resolution with respect to FIRST, in order to explore the morphology of these sourcesat different scales and wavelengths. Following the pilot study (Baldi et al. 2015), here we present VLA A-array radio observations for 18 sources at 1.5, 4.5 and 7.5 GHz reaching a resolution of ∼0.3 arcsec in order to: (i) study the extended emission, morphology and asymmetry; (ii) resolve the radio cores; and (iii) derive the radio spectral distributions.

The paper is organized as follows. In Section 2 we define the sample and present the new VLA observations for 18 sources. In Section 3 we analyse the radio and spectro-photometric properties of the sample, which are discussed in Section 4. The summary and conclusions to our findings are given in Section 5. We also present a revision of the FR0*CAT* sample in Appendix A.

2 THE SAMPLE AND THE VLA OBSERVATIONS

A total of 18 objects, whose main properties are listed in Table 1, were randomly extracted from the FR0*CAT* sample and observed with the VLA. More specifically, we formed groups of three or four FR0s located at small angular separations, in order to reduce the telescope overheads and the time needed for observations of the calibrators. All groups were included in the schedule, and five of them were actually executed. Because the observing strategy was based only on the location in the sky, this source selection does not introduce specific biases. The observed FR0s reside in the redshift range 0.019–0.050 and are representative of the whole FR0*CAT* sample in terms of radio and AGN power, as shown in Fig. 1. This figure also shows the large deficit of radio emission of FR0s when compared with the FRIs in the 3C sample, by a factor ranging from ∼30 to ∼1000 in the same range of bolometric AGN luminosity (represented by the [O III] line luminosity).

We obtained 8.67 h of observations with the VLA in its A-array configuration between 2016 December 27 and 2017 January 23. We observed the 18 objects in five separate scans, ranging from 1 to 2 h and including three or four sources. Similar to the observation strategy for the VLA pilot study of seven FR0s used in Baldi et al. (2015), the targets were observed in the L and C bands, splitting the exposure times in two. While the L-band configuration corresponds to the default 1-GHz-wide band centred at 1.5 GHz, the C band was modified in accordance with our purposes. We divided the available 2-GHz bandwidth into two subbands of 1 GHz centred at 4.5 and 7.5 GHz (hereafter the C1 and C2 bands, respectively). Each of the three bands was configured in seven subbands of 64 channels of 1 MHz. Each source was observed for ∼10 min in both the L and the C band, spaced out by the pointing to the phase calibrators for 2–4 min. The flux calibrator was 3C 286, observed for ∼6–7 min.

The data were calibrated by the CASA 5.0.0 pipeline v1.4.0, adding further manual flagging to remove low-level radio-frequency interferences and noisy scans in order to increase the general quality

Table 1. The sample of FR0s studied.

SDSS	Name	z	$L_{[O\,III]}$	M_{BH}	L_{NVSS}	L_{FIRST}	L_{core}
J090734.91+325722.9		0.049	39.33	7.7	39.60	39.52	<39.40
J093003.56+341325.3	MCG+06-21-042	0.042	39.93	8.4	39.31	39.24	<39.59
J093938.62+385358.6		0.046	39.59	8.1	38.65	38.62	39.22
J094319.15+361452.1	NGC 2965	0.022	39.85	7.9	39.10	39.05	<40.36
J101329.65+075415.6		0.046	39.86	8.7	38.76	38.68	39.18
J102544.22+102230.4		0.045	39.48	8.9	39.75	39.69	40.62
J104028.37+091057.1	NGC 3332	0.019	39.54	8.3	38.94	38.86	<39.19
J113637.14+510008.5	MCG+09-19-133	0.050	39.35	8.3	38.90	38.80	<38.71
J121329.27+504429.4	NGC 4187	0.031	40.12	8.7	39.50	39.49	40.09
J123011.85+470022.7	MCG+08-23-044	0.039	40.00	8.4	39.70	39.63	40.13
J150808.25+265457.6		0.033	39.36	8.1	38.87	38.85	39.38
J152010.94+254319.3	MCG+04-36-038	0.034	39.52	8.6	38.85	38.79	39.43
J153016.15+270551.0		0.033	39.71	8.2	38.69	38.66	39.93
J155951.61+255626.3	IC 4587	0.045	39.33	8.5	40.00	39.28	39.68
J162146.06+254914.4		0.048	39.61	8.1	38.87	38.79	<38.96
J162846.13+252940.9		0.040	39.65	8.5	39.15	39.14	39.87
J165830.05+252324.9		0.033	39.68	8.3	38.68	38.71	39vis41
J170358.49+241039.5	UGC 10678	0.031	39.66	8.8	39.03	38.84	<38.85

Note. Column description: (1) source SDSS name; (2) other name; (3) redshift; (4) logarithm of the [O III] line luminosity (erg s^{-1}); (5) logarithm of the BH mass ($M_{\odot}$); (6 and 7) logarithm of the radio luminosity from NVSS and FIRST (erg s^{-1}); (8) logarithm of the radio core luminosity (erg s^{-1}).

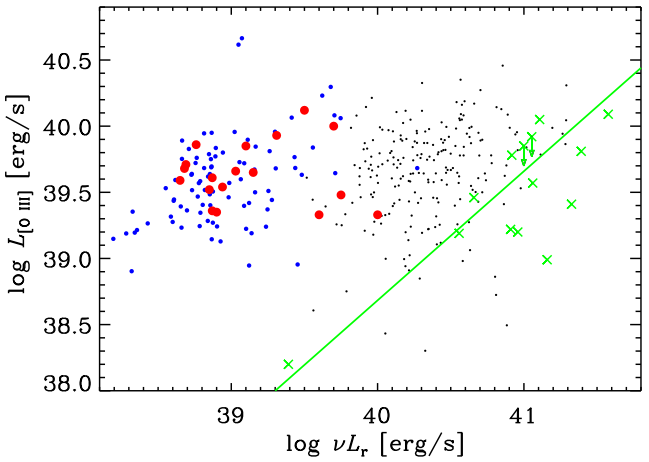

Figure 1. Total radio luminosity at 1.4 GHz from NVSS versus the [O III] line luminosity (erg s^{-1}). The large red dots represent the subsample of 18 galaxies presented in this paper; the medium blue points represent the 104 sources forming FR0*CAT*. The small black dots are the FRI radio galaxies of FRI*CAT* (Capetti et al. 2017a), while the green crosses are the FRIs in the 3C sample. The solid line represents the correlation between the line and radio luminosity derived for the 3CR/FRI sample (Buttiglione et al. 2010).

of the data. The final imaging process was performed with the AIPS (Astronomical Image Processing System) package according to standard procedures. The images were then produced in the L, C1 and C2 bands from the calibrated data using the task IMAGR. The angular resolutions reached in the three bands were, respectively, ∼1.7, 0.5 and 0.3 arcsec. We self-calibrated the maps of the sources with flux density $\gtrsim$5 mJy. The typical rms of the final images is ∼0.02 mJy, measured in background regions near the target. We measured the flux densities of the unresolved core components with the task JMFIT and the total radio emission from the extended sources with the task TVSTAT. In Table 2 we give the main parameters of the resulting images. Fig. 2 presents the maps of the extended radio sources with the radio contour levels listed in Table 3.

Table 2. Properties of the VLA images of the FR0 sample.

ID	Beam	rms	ID	Beam	rms
J0907+32	2.1 × 1.4	0.041	J1230+47	1.4 × 1.3	0.025
	0.7 × 0.5	0.014		0.5 × 0.5	0.020
	0.4 × 0.3	0.013		0.3 × 0.3	0.035
J0930+34	1.8 × 1.3	0.062	J1508+26	1.9 × 1.4	0.028
	0.7 × 0.5	0.021		0.5 × 0.5	0.013
	0.4 × 0.3	0.018		0.3 × 0.3	0.013
J0939+38	1.7 × 1.4	0.041	J1520+25	1.7 × 1.3	0.031
	0.7 × 0.5	0.012		0.5 × 0.5	0.013
	0.4 × 0.3	0.016		0.3 × 0.3	0.013
J0943+36	1.7 × 1.4	0.015	J1530+27	1.7 × 1.3	0.076
	0.7 × 0.5	0.018		0.5 × 0.5	0.020
	0.4 × 0.3	0.045		0.3 × 0.3	0.024
J1013+07	1.9 × 1.4	0.043	J1559+25	1.9 × 1.3	0.061
	0.8 × 0.5	0.012		0.6 × 0.5	0.023
	0.5 × 0.3	0.013		0.4 × 0.3	0.023
J1025+10	1.8 × 1.4	0.044	J1621+25	1.5 × 1.4	0.036
	0.7 × 0.5	0.017		0.6 × 0.5	0.013
	0.4 × 0.3	0.020		0.4 × 0.3	0.011
J1040+09	1.8 × 1.4	0.038	J1628+25	1.5 × 1.3	0.040
	0.6 × 0.5	0.017		0.6 × 0.5	0.019
	0.4 × 0.3	0.012		0.4 × 0.3	0.017
J1136+51	1.5 × 1.4	0.028	J1658+25	1.5 × 1.3	0.047
	0.5 × 0.5	0.012		0.5 × 0.5	0.016
	0.3 × 0.3	0.011		0.3 × 0.3	0.015
J1213+50	1.4 × 1.3	0.038	J1703+24	1.6 × 1.3	0.050
	0.5 × 0.5	0.027		0.5 × 0.5	0.013
	0.3 × 0.3	0.060		0.3 × 0.3	0.010

Note. Column description: (1)-(4) name; (2)-(5) beam size (arcseconds) at 1.4, 4.5 and 7.5 GHz in the three following rows; (3)-(6) rms (mJy $beam^{-1}$) at 1.4, 4.5 and 7.5 GHz in the three following rows.

3 RESULTS

The VLA observations show radio emission with flux densities in the three bands ranging between 1 and 281 mJy (with typical errors of 0.04 mJy in the L band and of 0.02 mJy in the two C bands). Most of the sources (14/18) appear unresolved down to

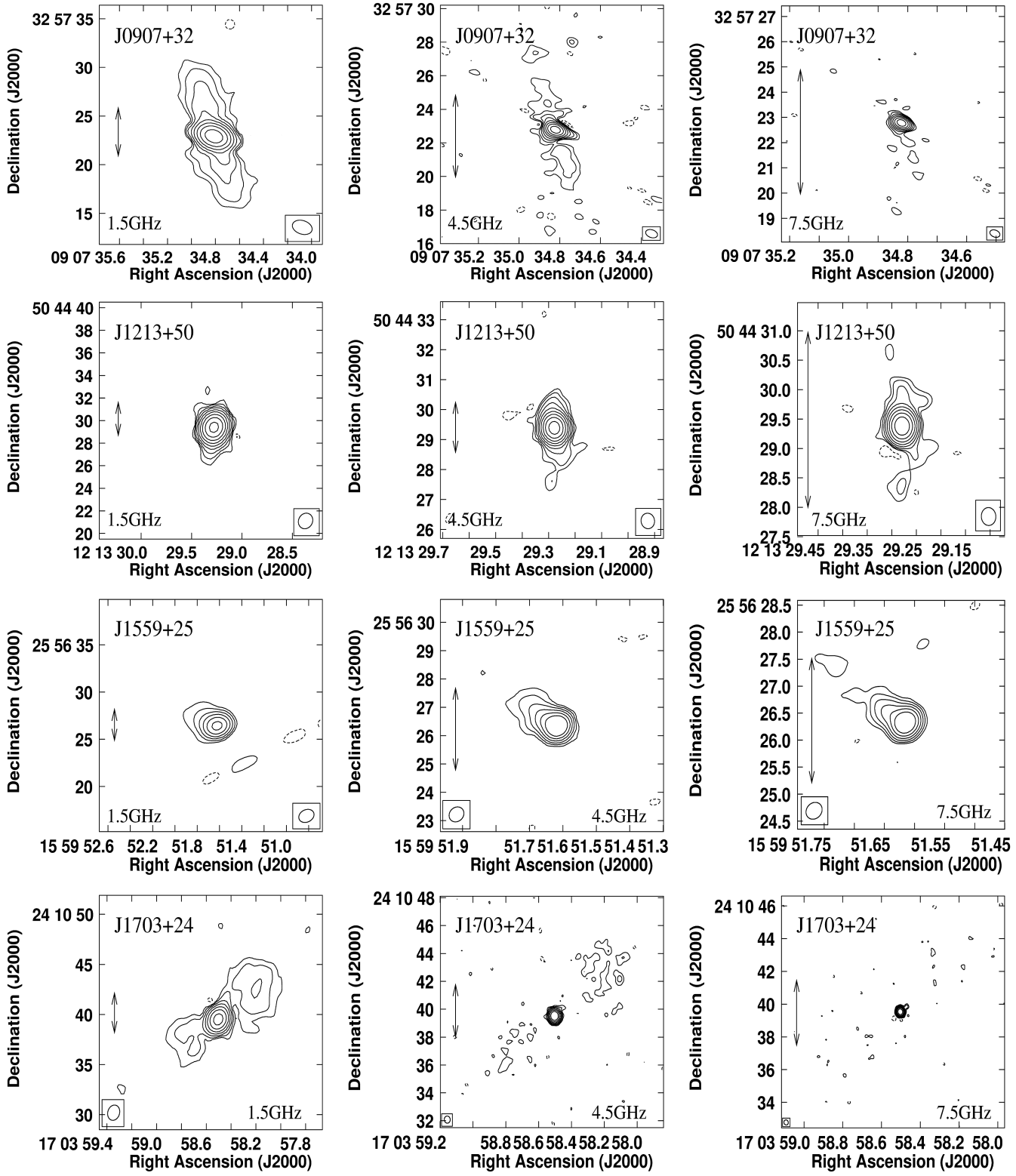

Figure 2. Radio images of the four FR0s in which we detected extended emission. The three columns show the images at 1.5 GHz (left), 4.5 GHz (centre) and 7.5 GHz (right), respectively. See Table 2 for angular resolutions and noise, and Table 3 for the list of contour levels. The arrowed lines represent a fixed scale bar for comparison for the three panels of each target.

Table 3. Contour levels (mJy beam^{-1}) for the sources presented in Fig. 2.

ID	Freq.	Contour levels
J0907+32	1.5	0.15 × (−1,1,2,4,8,16,32,64,128)
	4.5	0.05 × (−1,1,2,4,8,16,32,64,128)
	7.5	0.05 × (−1,1,2,4,8,16,32,64)
J1213+50	1.5	0.36 × (−1,1,2,4,8,16,32,64,128,256)
	4.5	0.20 × (−1,1,2,4,8,16,32,64,128,256)
	7.5	0.27 × (−1,1,2,4,8,16,32,64,128,256)
J1559+25	1.5	0.50 × (−1,1,2,4,8,16,32)
	4.5	0.12 × (−1,1,2,4,8,16,32)
	7.5	0.12 × (−1,1,2,4,8,16,32)
J1703+24	1.5	0.135 × (−1,1,2,4,8,16,32,64)
	4.5	0.035 × (−1,1,2,4,8,16,32,64)
	7.5	0.03 × (−1,1,2,4,8,16,32,64)

a resolution of $\sim$ 0.3 arcsec, which corresponds to 100–300 pc.[1] Four sources show radio emission extended over a few arcseconds, on a scale of 2–14 kpc (see Table 4 and Fig. 2). In J0907+32, two symmetric jets reach a distance of $\sim$7 arcsec ($\sim$14 kpc in the largest linear size, LLS). In J1213 + 50 the jets are best seen in the 4.5-GHz image, where they extend out to $\sim$1.5 arcsec (LLS $\sim$2 kpc) from the nucleus. Only one jet, $\sim$3 arcsec long (LLS $\sim$3 kpc), is detected in J1559+25. Finally, two diffuse radio structures are found in J1703 + 24, with an angular size of $\sim$14 arcsec (LLS $\sim$9 kpc). In Table 4 we also provide the total flux densities on the entire radio source. For the four extended sources, we estimated the jet counter-jet ratio, measuring the brightness ratio in two symmetric regions as near as possible to the nuclear emission by excluding the core brightness and considering the surface brightness at similar distances from the core. The brightness jet ratio ranges between $\sim$1 and 2, while one source is fully one-sided jetted (>8).

Our high-resolution VLA observations, obtained with a relatively short exposure time, might miss faint extended emission. In order to explore this possibility, we compared the observed total VLA 1.5-GHz flux densities with those measured by FIRST and NVSS at lower resolutions ($\sim$5 and $\sim$45 arcsec, respectively, see Table 4). The flux densities measured in the L band from our maps are generally consistent with those from the FIRST catalogue (derived from observations between 1994 and 1999 for our sources), an indication that we recovered most of the radio emission. Indeed, all but four sources show differences of less than 20 per cent over a time-scale of $\sim$20 yr. One of them (J1136+51) decreased in flux from 7.8 to 5.3 mJy. Three sources (namely J0943+36, 1025+10 and J1530 + 27) instead increased their flux densities, by a factor of between 1.5 and 3.2.

The 18 FR0s show a ratio between NVSS and FIRST flux densities very close to unity ($0.89 < F_{\rm NVSS}/F_{\rm FIRST} < 1.11$), with two exceptions. One is J1559+25, with a ratio of $\sim$5: this is the result of the presence of a second compact source with a FIRST flux density of 117 mJy located 28 arcsec to the west and blended with our target in the NVSS image. The second is J1703 + 24, with a ratio of 1.43: this is one of the FR0s with extended emission, suggesting that some extended emission is lost in the FIRST images.

We also obtained matched-beam radio maps[2] in order to derive the radio spectra at the three frequencies for all sources. The resolution-matched flux densities of the central components are reported in Table 4 and plotted in the radio spectra in Fig. 3. The typical flux errors for the central components are smaller than 0.1 mJy. For the brightest sources, exceeding $\sim$100 mJy, however, they can be as high as 0.5 mJy. We do not report them in the table for the sake of clarity.

The spectral indices α between 1.5 and 4.5 GHz ($F_\nu \propto \nu^\alpha$) cover a broad range, from $\sim$1 to –0.2: most spectra are flat ($-0.2 < \alpha < 0.4$ is measured for 11 objects), six are steep ($0.49 < \alpha < 1.03$). In one case (J0943+36), the spectrum is strongly inverted, with $\alpha = -0.6$. If we consider the spectral indices measured between the two adjacent bands, we typically observe a spectral steepening at 7.5 GHz, with a median difference between the two indices of $\Delta\alpha \sim 0.16$. We also note that four flat-spectrum sources (1025+10, 1530+27, 1628+25, 1658 + 25) have slightly convex radio spectra: the flux density at 4.5 GHz is typically $\sim$20 per cent higher than that at 1.5 GHz and 15 per cent higher than that at 7.5 GHz.

Interestingly, the results of very-long-baseline interferometry (VLBI) observations for four of the FR0s studied here have been recently presented by Cheng & An (2018). J0943+36, the inverted-spectrum source, shows an unresolved VLBI core with an inverted spectrum and significant variability, with a flux density increasing from 0.17 to 0.25 Jy over 4 yr. J1213+50, a twin-sided jet FR0, shows a similar morphology but on a milliarcsecond scale and perpendicular to the VLA jets. J1230+47, a flat-spectrum FR0, shows twin jets on a milliarcsecond scale with VLBI. J1559 + 25, the one-sided FR0, appears similarly one-sided on a milliarcsecond scale with VLBI, with no sign of variability (<20 per cent).

One of the aims of this study is the measurement of the radio core. In the four extended sources a compact central component is always clearly visible. However, the spectrum of the central source of, for example, J0907 + 32 is very steep ($\alpha \sim 1$), indicating a substantial contribution from optically thin, extended emission. We must then rely on the radio spectra to isolate the core emission. We considered as core-dominated the 11 sources with a central component characterized by a flat spectrum ($\alpha \lesssim 0.4$). For the remaining objects the 7.5-GHz flux density is adopted as the upper limit to the core. In Baldi et al. (2015) we noticed several sources with a flattening of the radio spectrum between 4.5 and 7.5 GHz with respect to that measured between 1.5 and 4.5 GHz and interpreted this behaviour as the emergence of a flat core at the higher frequencies. In the observations we are presenting here, there is no clear evidence of a flattening of the radio spectra at 7.5 GHz: the extrapolation of the spectra derived from 1.5 to 4.5 GHz agrees or slightly over-predicts the actual measurement at 7.5 GHz by $\sim$20 per cent.

The distribution of core dominance of our sources, R, defined as the ratio between the nuclear emission at 7.5 GHz and the total NVSS flux density at 1.4 GHz[3], is presented in Fig. 4. The 11 sources with a flat spectrum have $-0.4 \lesssim \log R \lesssim 0.5$. The upper limits on log$R$ for those with a steep spectrum are in the range −0.9 to −0.4. This distribution is significantly different from that

[1] In Appendix A, we also show the radio maps at the three frequencies of IC 711, originally included in the FR0*CAT* sample (and observed in this VLA project) but subsequently discarded based on the presence of extended emission visible in the NVSS image of the source.

[2] We matched the C-band radio images at the resolution obtained in the L band by using the parameter *uvtaper* in the IMAGR task in AIPS.

[3] Except for J1559 + 25, for which we used the FIRST data because of the contamination to the NVSS flux density from the nearby source.

Table 4. Radio properties of the FR0 sample.

Name	NVSS	FIRST	$F_{1.5}$	$F_{4.5}$	$F_{7.5}$	$F_{1.5,tot.}$	Morph.	Size	Jet ratio
J0907+32	46.9	42.9	32.7	10.61	5.92	42.5	Twin-jets	14 kpc	1.3 ± 0.23
J0930+34	33.1	30.8	28.73	16.77	12.51				
J0939+38	6.1	6.2	5.87	5.20	4.48				
J0943+36	75.1	74.9	133.3	257.8	280.4				
J1013+07	7.8	7.0	8.08	5.51	4.02				
J1025+10	76.6	75.7	113.6	129.6	116.2				
J1040+09	68.5	64.7	68.0	35.1	25.44				
J1136+51	9.0	7.8	5.33	2.29	1.16				
J1213+50	96.5	102.7	122.7	85.8	74.0	133.0	Two jets	2 kpc	2.0 ± 0.7
J1230+47	93.8	87.4	89.0	65.0	51.2				
J1508+26	20.3	20.5	18.94	15.62	12.63				
J1520+25	18.3	17.1	17.09	16.13	13.48				
J1530+27	13.3	13.4	42.8	52.9	45.1				
J1559+25	155.9	29.2	20.78	15.31	13.30	24.5	One jet	3 kpc	>8
J1621+25	9.1	8.4	7.44	3.44	2.22				
J1628+25	25.2	27.4	27.22	30.59	26.40				
J1658+25	13.1	14.8	13.97	14.91	13.65				
J1703+24	32.7	22.8	12.87	6.46	4.29	17.7	Two lobes	9 kpc	1.0 ± 0.4

Note. Column description: (1) source name; (2) and (3) NVSS and FIRST 1.4-GHz flux density (mJy); (4), (5) and (6) fluxes of the nuclear components from matched-beam images at the three observing frequencies (mJy); (7) total flux at 1.5-GHz flux density (mJy); (8) morphology for the extended sources; (9) largest linear size; and (10) brightness ratio between the opposite structures for the extended sources.

of 3CR/FRIs (with a >99.9 per cent probability, according to a Kolmogorov–Smirnoff test), while it is not distinguishable from the *R* distribution of CoreGs and the other FR0s studied in the previous VLA project (Baldi & Capetti 2010; Baldi et al. 2015).[4]

We can now include our sources in the $L_{core}(=L_{7.5GHz})$ versus $L_{[O\,III]}$ plane, similarly to in Baldi et al. (2015) for the VLA FR0 pilot study. This diagnostic plot compares the radio-core energetics with the line luminosity, adopted as a proxy for the AGN luminosity (Heckman et al. 2004). The FR0s lie in the region populated by the lower-luminosity 3CR/FRIs and follow the same core–line relationship as found for FRIs and CoreGs. This relationship further strengthens the similarity between the nuclei of FR0s and FRIs. However, we recall that for seven of them we only derived upper limits to their radio-core flux densities because of the lack of a clear flat-spectrum unresolved core. Although the point scatter of FR0s is consistent with that of FRIs, the presence of upper limits on the core measurements in the correlation challenges the FR0–FRI similarity scenario.

4 DISCUSSION

Despite the fact that FR0s have the same properties as FRI radio galaxies from the nuclear and host points of view, FR0s differ from the other FR classes in their remarkable lack of significant extended radio emission, and in being dominated by a subkiloparsec-scale flat-spectrum component. In Baldi et al. (2015) and Baldi et al. (2018a) we discussed various scenarios to interpret this unique feature of FR0s and we now review them in the light of the results obtained with the new VLA observations.

Baldi et al. (2018a) concluded that a scenario in which all FR0s are young radio sources that will eventually evolve into extended radio sources is not consistent with the relative number densities of these classes. Thanks to new high-resolution observations, we can further test this possibility, by exploring the distribution of radio sizes of FR0s. In Fig. 6 we show the size distribution of all 182 SDSS/NVSS LEG radio galaxies with z <0.05, 104 of which are included in FR0*CAT*. The fraction of FR0s unresolved in the VLA observations is ∼78 per cent, for which we set a conservative size limit of 1 kpc (represented by the arrow in the left panel of Fig. 6), and they represent ∼44 per cent of the whole population of radio-emitting AGNs within this volume. The remaining sources extend up to ∼100 kpc, and about one-third of them are FRIs, part of the FRI*CAT* and sFRI*CAT*[5] samples (Capetti et al. 2017a). In the right panel of this figure we present the number of objects in each bin, divided by the bin size in kiloparsecs. As already discussed in Baldi et al. (2018a), in the case of a constant expansion speed all bins should be equally populated. Conversely, the number density of sources with size $\lesssim$1 kpc exceed by ∼2 orders of magnitude that of the extended sources, indicating that FR0s do not generally grow to become large radio galaxies.

The distribution of sizes also sets strong constraints of the interpretation that FR0s are short-lived recurrent sources. As we noted in Baldi et al. (2015), the results obtained by Shin, Ostriker & Ciotti (2012) indicate that the more massive galaxies spend a larger fraction of their time in active states than satellite galaxies. The possibility that this is the origin of the strong peak in the size distribution appears to be rather contrived considering the relatively small differences in host galaxy masses between FR0s and FRIs, on average only a factor 1.6 and with a substantial overlap between the two classes (Baldi et al. 2018a; Miraghaei & Best 2017). Nevertheless, it is the case that a low/moderate-amplitude radio flux density variation has been detected for a few FR0s over a

[4]We estimated *R* as the ratio between the 7.5-GHz core emission and the total 1.4-GHz flux density, while for the 3CR/FRI sources we used the 5-GHz core flux density against the 1.4-GHz total flux density. However, because the radio core emission generally has a flat spectrum, this quantity is only weakly dependent on the frequency used for the core measurement and this comparison is robust.

[5]FRI radio galaxies selected in FIRST with radio sizes larger than 30 kpc (FRI*CAT*) and between 10 and 30 kpc (sFRI*CAT*).

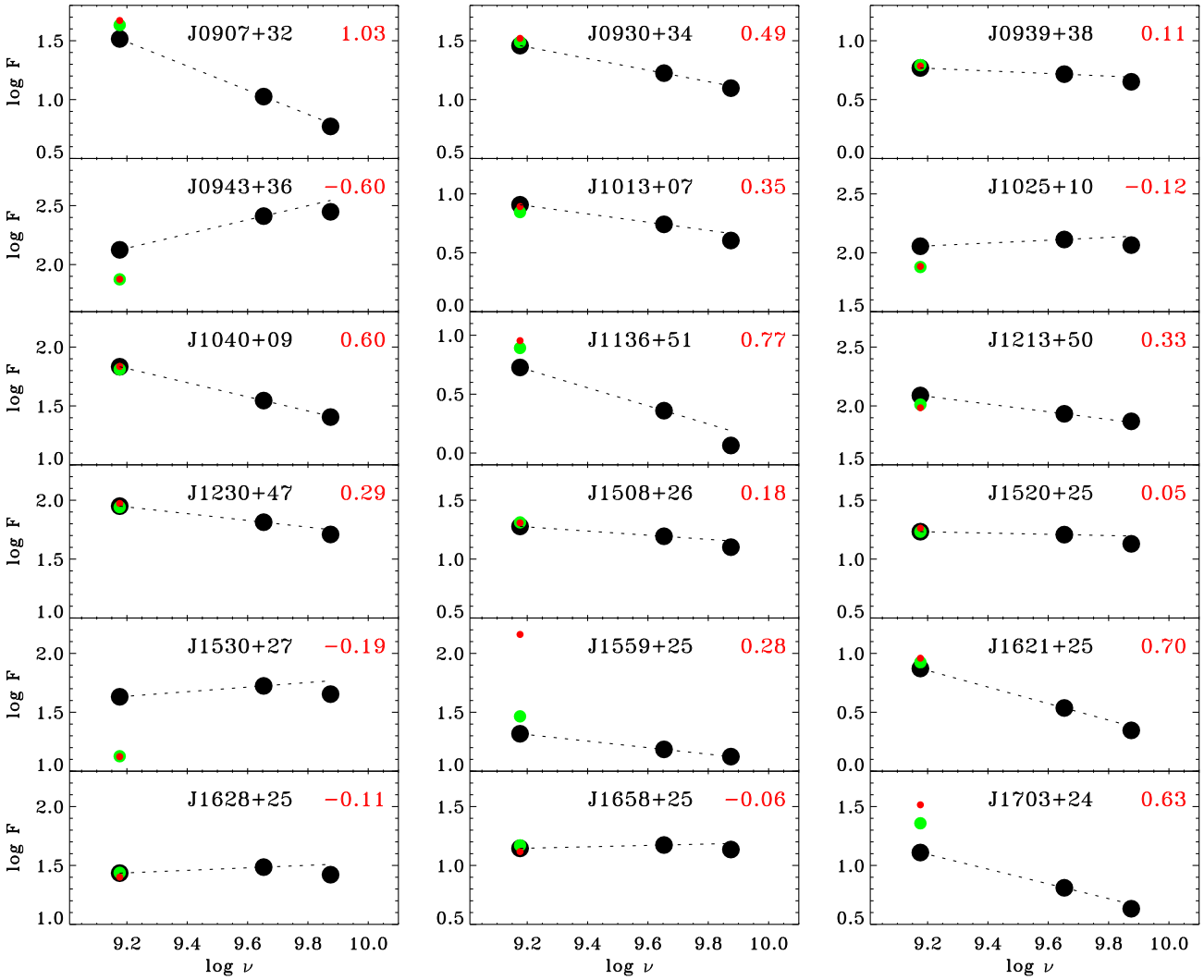

Figure 3. Radio spectra of the central components of the 18 FR0s observed with the VLA. The black dots are the VLA data, while the red and green dots are the NVSS and FIRST flux densities, respectively. The dashed line represents the power law obtained from the 1.5- and 4.5-GHz VLA measurements; its slope is reported at the top right of each panel. Flux densities are in mJy, frequencies are in Hz.

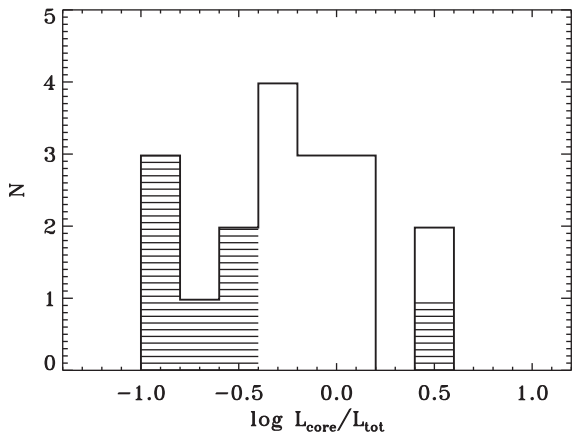

Figure 4. Distribution of core dominance R, namely the ratio between the flux density of the central component at 7.5 GHz and the NVSS flux density at 1.4 GHz. The hatched histogram corresponds to upper limits on R for the sources with no radio-core detection.

time-scale of years (Cheng & An 2018). This variability is not necessarily associated with a nuclear recurrence, but is a phenomenon expected within an evolutionary scenario of the source (Morganti 2017).

Another scenario for the origin of FR0s is related to the jet-launching region. The similar nuclear luminosities of FR0s and FRIs and the FR0 radio morphologies we observed suggest that within the radio core, less than 1 kpc, the jets of FR0s should be relativistic (Cheng & An 2018). However, at larger scales (>1 kpc), we envisage that the lower jet Γ factors of FR0s than in FRIs reduce the jet ability to penetrate the host's interstellar medium and transforming the relativistic jets to turbulent flow not far outside the optical core of the galaxy, as seen in nearby FRI radio galaxies (e.g. Killeen, Bicknell & Ekers 1986; Venturi et al. 1993; Bicknell 1995). However, no evidence of deceleration sites along the jet at various scales has been observed for our FR0 sources. We can test the possibility of a jet deceleration and determine the bulk jet speed by measuring the sidedness of jets in FR0s and comparing it with that of FRIs. By considering this new data set together with the results of the pilot program, there are now five FR0s with fairly

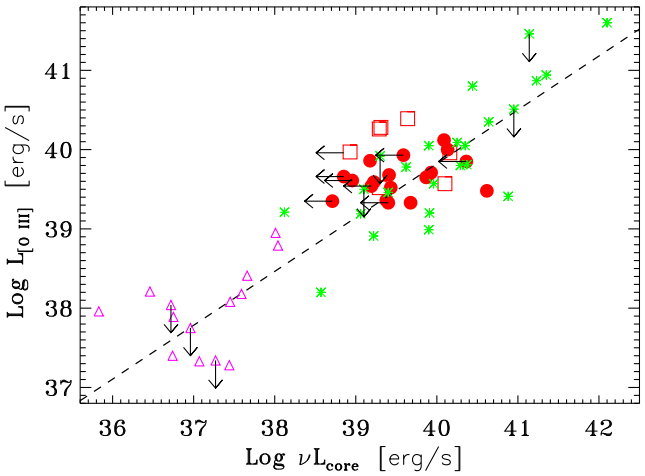

Figure 5. Core radio power versus [O III] line luminosity (erg s^{-1}) for CoreGs (pink triangles), 3CR/FRI radio galaxies (green asterisks), and FR0s (red dots) from this study and the seven FR0s (red squares) from the VLA pilot study (Baldi et al. 2015). The line indicates the best linear correlation found for 3CR/FRIs.

symmetrical extended or slightly sided structures (jet brightness ratio 1–2; J0907+32, J1213+50, J1703 + 24 in this work, and ID 547 and ID 590 from Baldi et al. 2015). We also found one highly asymmetric source, but the minimum jet Lorentz factor to obtain the observed flux ratio between the jet and counter-jet of $\gtrsim$8 is only $\Gamma \gtrsim 1.1$, which is not necessarily indicative of a highly relativistic jet. From the comparison between our VLA and VLBI images from Cheng & An (2018) for five FR0s, we learnt that, when observed, subkiloparsec-scale jets are typically present also at milliarcsecond scales. However, for our source (J1213+504) the milliarcsecond-scale jets appear perpendicular to those observed with the VLA, possibly as a result of jet procession, while in one compact FR0 (J1230 + 47), two parsec-scale twin jets emerge, pointing to a subrelativistic jet speed on sizes smaller than that probed by the VLA. An inferred mildly relativistic jet bulk speed on subkiloparsec scales is in agreement with the Doppler boosting factors estimated by Cheng & An (2018) from VLBI observations. The modelling of the multiband spectrum of the first FR0 detected in the γ-ray with *Fermi* (Grandi, Capetti & Baldi 2016) with standard beamed and misaligned jet models (Maraschi & Tavecchio 2003; Ghisellini, Tavecchio & Chiaberge 2005) produces a bulk jet Γ factor of 2–10 (Tavecchio et al. 2018). Clearly, the statistics on the jets asymmetries in FR0s is still insufficient to draw a firm conclusion on their speed, but evidence for a mildly relativistic jet speed is increasing.

Another way to measure the jet speed is to consider the dispersion of the core powers with respect to a quantity independent of orientation, such as the emission-line luminosity, see Fig. 5. Because there might be a substantial level of intrinsic scatter, this approach can provide us with an *upper limit* on the jet Γ. Owing to the presence of a significant fraction of non-detections of flat cores, however, we can only derive a *lower limit* to the core dispersion. Higher-frequency observations are needed to isolate the core emission also in the sources with steep spectra and to fully exploit this method.

We must also mention that a different matter content of the FR0 jets from the other FR classes might account for the reduced jet extension observed in FR0s. Lighter jets, possibly composed mainly of electron–positron pairs (Ghisellini 2012), would correspond to a much lower jet power, again hampering the formation of large-scale radio structures with respect to what is predicted by a leptonic model (Maraschi & Tavecchio 2003).

While the majority of FR0s conform with the idea that they are compact flat-spectrum sources, some of them show steep spectra. Interestingly, the fraction of flat and steep sources in our sample (with a two to one ratio) is the same as found by Sadler et al. (2014) in their sample of FR0 LEGs, despite the different selection criteria. FR0s certainly are a mixed population of low-power radio sources, one expected contaminant being a small population of genuinely young FRIs, as also suggested by Cheng & An (2018).

We also note that four sources show a slightly convex radio spectrum and one source (J0943 + 36) has an inverted spectrum, similar to what is seen in GHz-peaked sources (GPSs, Peacock & Wall 1982). Nevertheless, VLBI observations (Cheng & An 2018) did not resolve milliarcsecond-scale double lobes, the typical morphology that would be expected for this class of radio sources. Therefore, the particular radio behaviour of J0943 + 36 requires more attention to investigate whether its compactness and spectrum reconciles with this source being a young radio galaxy, which expands at a very low rate owing to its much lower power with respect to GPSs (O'Dea 1998) or, instead, is consistent with what is expected for young FRIs.

5 SUMMARY AND CONCLUSIONS

We presented new VLA observations at array A at three frequencies, 1.5, 4.5 and 7.5 GHz, for a sample of 18 FR0 radio galaxies selected from the FR0*CAT* sample. At the highest angular resolution (∼0.3 arcsec), most of the sources are still unresolved, with ∼80 per cent of the total radio emission enclosed in the core (i.e. they are more core-dominated than FRIs by a factor of ∼30). Only four objects show extended emission up to 14 kpc, with various morphologies: one- and two-sided jets, and double lobes. Six have steep radio spectra, one shows an inverted spectrum, and 11 have flat cores. Four of the flat-spectrum cores in FR0s are actually slightly convex, with a small steepening between 4.5 and 7.5 GHz with respect to the slope measured at lower frequencies.

For 11 of the sources, where a radio core is detected, the core and emission-line luminosities are correlated, following the relationship that is valid for FRI and CoreG radio galaxies at high and low luminosities, respectively. However, for seven sources, owing to their steep spectra and morphology, we can give only an upper limit to the radio-core luminosity, which is still in agreement with the correlation. More high-resolution data are necessary to isolate their core components. By adding the seven FR0s studied in a previous VLA exploratory pilot study (Baldi et al. 2015), we confirm the similarity between the radio cores of FR0s and FRIs and the absence of a strong beaming effect in the FR0 cores.

The size distribution of nearby $z < 0.05$ RL AGNs shows, thanks to the new observations, a strong peak for sources smaller than ∼1kpc. This rules out the possibility that FR0s are young sources that will all evolve into more extended radio galaxies, and it also disfavours the interpretation that they are recurrent sources, with very short periods of activity. The most likely possibility is that FR0s are associated with jets that are mildly relativistic at subkiloparsec scales.

The combination of the high resolution, large collecting area, and wide frequency range of the new generation of radio telescopes (e.g. SKA, ngVLA, LOFAR) will enable us to respond to the increas-

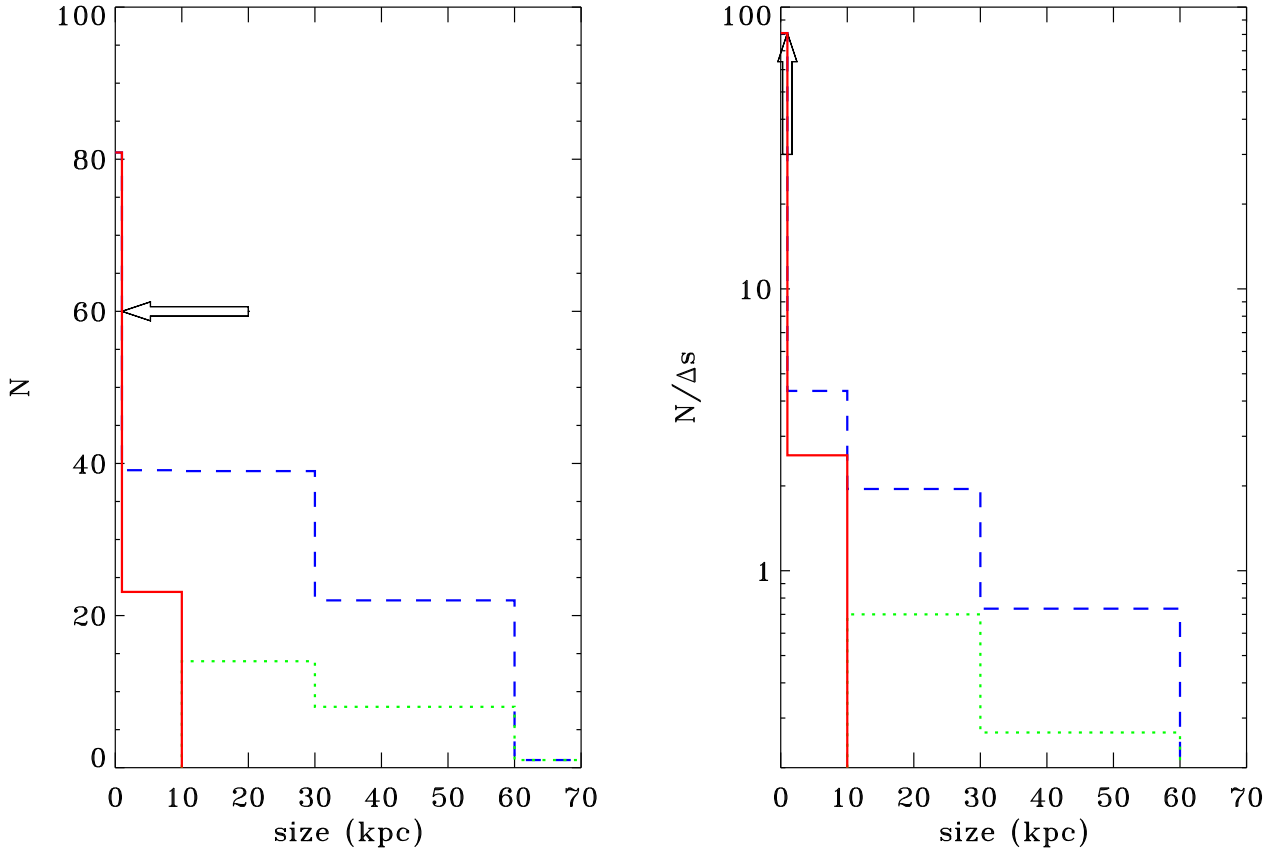

Figure 6. (Left) Size distribution of SDSS/NVSS LEG radio galaxies with $z < 0.05$ (dashed blue histogram). We separate the contribution of FRIs (dotted green line) and FR0s (solid red line): the first bin contains the 14 unresolved FR0s, with a size limit of <1 kpc (scaled by our VLA coverage of the FR0*CAT* sample, i.e. by 104/14); the second bin represents the FR0s found to be extended from the VLA observations. (Right) Size distribution normalized by the bin size in kiloparsecs (note the logarithmic scale of the vertical axis). The first bin is the lower limit corresponding to the unresolved FR0s.

ing interest in low-power radio sources (Nyland et al. 2018), and, consequently, in FR0s (Whittam et al. 2017). The advent of larger radio surveys will provide the opportunity to study the parsec-scale emission of FR0s and to test whether their jets have a smaller bulk jet speed than the other FR classes on firmer statistical grounds, by expanding the size of the observed sample with high-quality radio observations. Higher-frequency observations are also needed to isolate the core emission in sources in which the radio spectrum is steep and to detect their jets. Equally, lower-frequency observations will be very useful in establishing whether among them there are other inverted-spectrum sources. This in turn will indicate the nature of FR0s: they have slow jets or they are young radio sources?

ACKNOWLEDGEMENTS

The National Radio Astronomy Observatory is a facility of the National Science Foundation operated under cooperative agreement by Associated Universities, Inc. RDB acknowledges the support of STFC under grant ST/M001326/1. We thank Francesca Panessa, Graziano Chiaro and Matt Malkan for a helpful discussion on the nature of compact radio sources. We also thank the reviewer for the useful comments, which helped us to improve the quality of the manuscript.

REFERENCES

Baldi R. D., Capetti A., 2009, A&A, 508, 603
Baldi R. D., Capetti A., 2010, A&A, 519, A48
Baldi R. D., Capetti A., Giovannini G., 2015, A&A, 576, A38
Baldi R. D., Capetti A., Giovannini G., 2016, Astron. Nach., 337, 114
Baldi R. D., Capetti A., Massaro F., 2018a, A&A, 609, A1
Baldi R. D. et al., 2018b, MNRAS, 476, 3478
Balmaverde B., Capetti A., 2006, A&A, 447, 97
Banfield J. K. et al., 2015, MNRAS, 453, 2326
Bennett A. S., 1962, Mem. R. Astron. Soc., 68, 163
Best P. N., Heckman T. M., 2012, MNRAS, 421, 1569
Best P. N., Kauffmann G., Heckman T. M., Ivezić Ž., 2005, MNRAS, 362, 9
Bicknell G. V., 1995, ApJS, 101, 29
Bodo G., Mamatsashvili G., Rossi P., Mignone A., 2013, MNRAS, 434, 3030
Buttiglione S., Capetti A., Celotti A., Axon D. J., Chiaberge M., Macchetto F. D., Sparks W. B., 2010, A&A, 509, A6
Capetti A., Massaro F., Baldi R. D., 2017a, A&A, 598, A49
Capetti A., Massaro F., Baldi R. D., 2017b, A&A, 601, A81
Cheng X.-P., An T., 2018, ApJ, 863, 155
Colla G., Fanti C., Fanti R., Gioia I., Lari C., Lequeux J., Lucas R., Ulrich M. H., 1975, A&AS, 20, 1
Ekers R. D., Ekers J. A., 1973, A&A, 24, 247
Falcke H., Nagar N. M., Wilson A. S., Ulvestad J. S., 2000, ApJ, 542, 197
Filho M. E., Barthel P. D., Ho L. C., 2000, ApJS, 129, 93
Filho M. E., Barthel P. D., Ho L. C., 2002, ApJS, 142, 223
Ghisellini G., 2011, AIPC, 1381, 180

Ghisellini G., 2012, MNRAS, 424, L26
Ghisellini G., Tavecchio F., Chiaberge M., 2005, A&A, 432, 401
Giroletti M., Giovannini G., Taylor G. B., 2005, A&A, 441, 89
Grandi P., Capetti A., Baldi R. D., 2016, MNRAS, 457, 2
Heckman T. M., Kauffmann G., Brinchmann J., Charlot S., Tremonti C., White S. D. M., 2004, ApJ, 613, 109
Heeschen D. S., 1970, AJ, 75, 523
Killeen N. E. B., Bicknell G. V., Ekers R. D., 1986, ApJ, 302, 306
Lukic V., Brüggen M., Banfield J. K., Wong O. I., Rudnick L., Norris R. P., Simmons B., 2018, MNRAS, 476, 246
Maraschi L., Tavecchio F., 2003, ApJ, 593, 667
Miraghaei H., Best P. N., 2017, MNRAS, 466, 4346
Morganti R., 2017, Nat. Astron., 1, 596
Nagar N. M., Falcke H., Wilson A. S., Ho L. C., 2000, ApJ, 542, 186
Nagar N. M., Falcke H., Wilson A. S., Ulvestad J. S., 2002, A&A, 392, 53
Nyland K., Young L. M., Wrobel J. M., Sarzi M., Morganti R., al., 2016, MNRAS, 458, 2221
Nyland K., Harwood J. J., Mukherjee D., Jagannathan P., Rujopakarn W., Emonts B., al., 2018, ApJ, 859, 23
O'Dea C. P., 1998, PASP, 110, 493
Peacock J. A., Wall J. V., 1982, MNRAS, 198, 843
Rogstad D. H., Ekers R. D., 1969, ApJ, 157, 481
Sadler E. M., Ekers R. D., Mahony E. K., Mauch T., Murphy T., 2014, MNRAS, 438, 796
Shin M.-S., Ostriker J. P., Ciotti L., 2012, ApJ, 745, 13
Slee O. B., Sadler E. M., Reynolds J. E., Ekers R. D., 1994, MNRAS, 269, 928
Tavecchio F., Righi C., Capetti A., Grandi P., Ghisellini G., 2018, MNRAS, 475, 5529
Torresi E., Grandi P., Capetti A., Baldi R. D., Giovannini G., 2018, MNRAS , 476, 5535
Vallee J. P., Roger R. S., 1987, AJ, 94, 1
Vallee J. P., Wilson A. S., 1976, Nature, 259, 451
Venturi T., Giovannini G., Feretti L., Comoretto G., Wehrle A. E., 1993, ApJ, 408, 81
Wall J. V., Peacock J. A., 1985, MNRAS, 216, 173
Whittam I. H., Riley J. M., Green D. A., Jarvis M. J., 2016, MNRAS, 462, 2122
Whittam I. H., Jarvis M. J., Green D. A., Heywood I., Riley J. M., 2017, MNRAS, 471, 908
Wrobel J. M., Heeschen D. S., 1991, AJ, 101, 148

APPENDIX: THE CASE OF IC 711 AND AN UPDATE OF THE FR0*CAT*

Most of the 108 sources in the FR0*CAT* catalogue show a ratio between the FIRST and NVSS flux densities of between 0.8 and 1.2, indicating that, in general, in FR0s there is no significant amount of extended low-brightness radio emission lost as a result of the missing short baselines of the FIRST observations. However, individual exceptions might exist. In Fig. A1 we present the images obtained as part of our program of VLA observations of SDSS J113446.55 + 485721.9, which shows a pair of bent asymmetric jets extending for ∼90 arcsec from the radio core. This source, also known as IC 711, is actually the longest head–tail radio source known (Vallee & Wilson 1976), extending over ∼500 kpc (Vallee & Roger 1987). Its extended nature is clearly seen also in the NVSS image (see Fig. A2).

The NVSS images were not used for the FR0 selection because of their low spatial resolution (45 arcsec) and the resulting high level of confusion. Nonetheless, the case of IC 711 indicates that they can still be used to improve the source morphological classification. We then retrieved the NVSS images of all 108 FR0s in FR0*CAT*, looking for extended emission. Elongations in the iso-contours are rather common, usually extending in just one direction. As expected, in most cases this is the result of confusion, owing to the presence of a nearby radio source, well visible in the FIRST images. Nonetheless, there are four sources in which the radio emission is clearly extended. Their NVSS images are shown in Fig. A2. These sources (namely SDSS J112039.95+504938.2, SDSS J113446.55+485721.9 aka IC 711, SDSS J160616.02+181459.8 and SDSS J162549.96 + 402919.4) are not genuine compact FR0s and should be removed from the FR0*CAT* catalogue, which now contains 104 sources.

Regarding IC 711, the core flux densities measured from the VLA observations are 25.92 ± 0.03 at 1.5 GHz, 24.30 ± 0.02 at 4.5 GHz, and 23.23 ± 0.01 at 7.5 GHz, showing a flat spectrum with $\alpha = -0.07$. In this source the jets are highly asymmetric in the innermost regions, but their brightness ratio decreases at larger distances, possibly owing to a deceleration from relativistic to subsonic (Bicknell 1995).

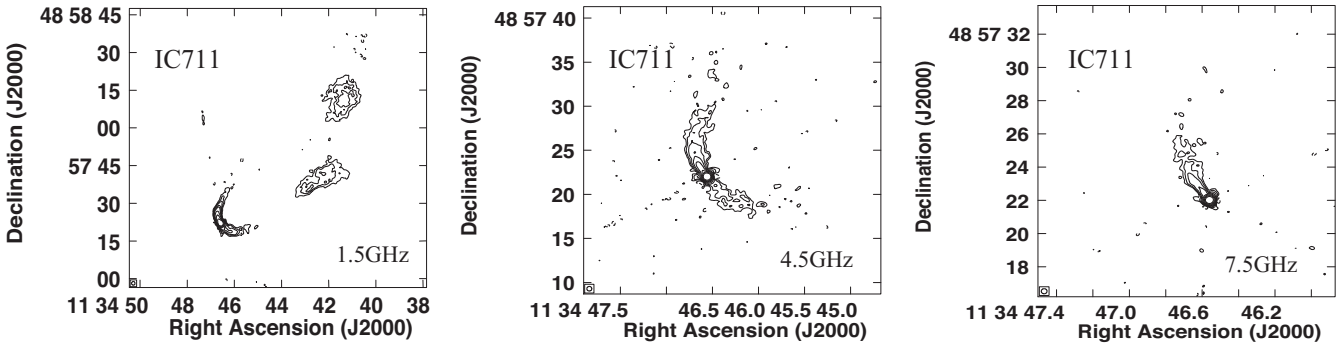

Figure A1. VLA images of SDSS J113446.55 + 485721.9 (aka IC 711) at 1.5 , 4.5 and 7.5 GHz (left, middle and right panels, respectively). Contour levels are drawn at: 0.17 × (−1,1,1.5,2,3,4,8,16,32) mJy beam^{-1} at 1.5 GHz; 0.04 × (−1,1,2,4,8,16,32,64,128) mJy beam^{-1} at 4.5 GHz; 0.05 × (−1,1,2,4,8,16,32,64,128) mJy beam^{-1} at 7.5 GHz.

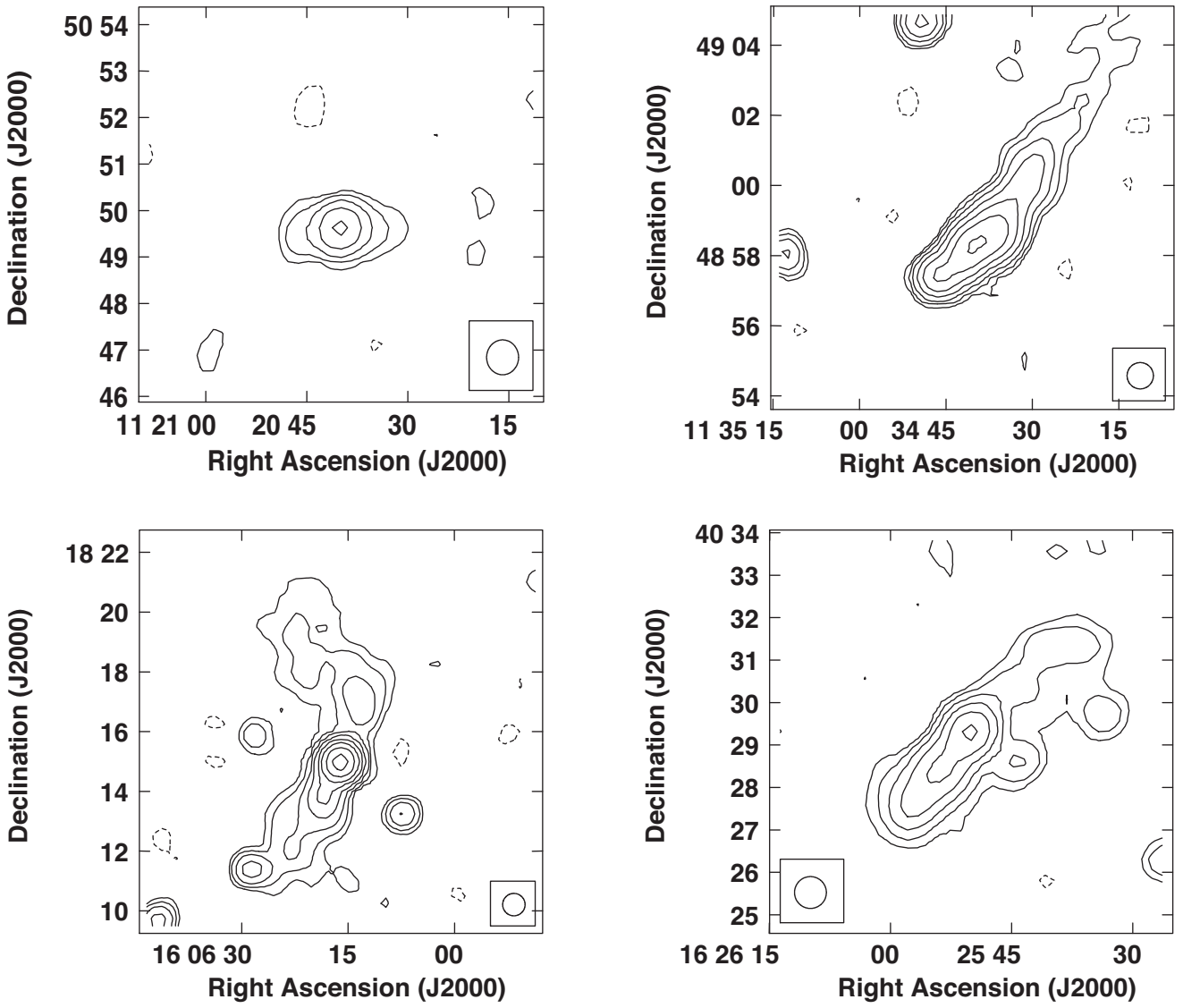

Figure A2. NVSS images of the four sources erroneously included in the FR0*CAT* catalogue but clearly showing extended radio emission and now excluded from the catalogue: from top left to bottom right panel, SDSS J1120+50, SDSS J1134+48 aka IC 711, SDSS J1606+18 and SDSS J1625 + 40. The contour levels of the maps are (−1, 1, 2, 4, 8, ...) mJy beam^{-1}.

This paper has been typeset from a TEX/LATEX file prepared by the author.